PHYSICAL REVIEW B **90**, 161103(R) (2014)

# Structural and magnetic dynamics in the magnetic shape-memory alloy $Ni_2MnGa$

S. O. Mariager,[1,*] C. Dornes,[2] J. A. Johnson,[1] A. Ferrer,[2] S. Grübel,[1] T. Huber,[2] A. Caviezel,[1] S. L. Johnson,[2] T. Eichhorn,[3] G. Jakob,[3] H. J. Elmers,[3] P. Beaud,[1] C. Quitmann,[1,†] and G. Ingold[1,‡]

[1]*Swiss Light Source, Paul Scherrer Institut, 5232 Villigen, Switzerland*

[2]*Institute for Quantum Electronics, ETH Zurich, 8093 Zürich, Switzerland*

[3]*Institut für Physik, Johannes Gutenberg-Universität Mainz, 5128 Mainz, Germany*

(Received 23 May 2014; revised manuscript received 26 August 2014; published 10 October 2014)

Magnetic shape-memory Heusler alloys are multiferroics stabilized by the correlations between electronic, magnetic, and structural order. To study these correlations we use time-resolved x-ray diffraction and magneto-optical Kerr effect experiments to measure the laser induced dynamics in a Heusler alloy $Ni_2MnGa$ film and reveal a set of time scales intrinsic to the system. We observe a coherent phonon which we identify as the amplitudon of the modulated structure and an ultrafast phase transition leading to a quenching of the incommensurate modulation within 300 fs with a recovery time of a few ps. The thermally driven martensitic transition to the high temperature cubic phase proceeds via nucleation within a few ps and domain growth limited by the speed of sound. The demagnetization time is 320 fs, which is comparable to the quenching of the structural modulation.

DOI: 10.1103/PhysRevB.90.161103 PACS number(s): 75.80.+q, 63.20.kd, 78.47.J−, 81.30.Kf

Multiferroic materials which exhibit large responses to electromagnetic and stress fields are of great interest for novel technical applications. To guide their rational design the microscopic origin of their functional properties must be understood, which requires methods that can disentangle the interplay between electronic, magnetic, and structural degrees of freedom. A prototypical example is the optimization of ferromagnetic $X_2YZ$ Heusler alloys, where one class shows novel functional properties such as magnetic shape-memory and magnetocaloric effects due to the coexistence of ferromagnetism and a structural martensitic (MT) transition [1], and another class is half metallic and suitable for spintronic applications [2]. $Ni_2MnGa$ is the classical Heusler magnetic shape-memory alloy with a magnetically induced strain of up to 10% arising from the interplay between magnetic and structural domains in the twinned low temperature MT phase [1,3–5]. The structure of the MT phase changes with alloy composition [6], but the modulated phases (commonly labeled 5M and 7M) [7,8] displaying magnetic shape memory only exist if the MT transition temperature $T_{MT}$ is lower than the Curie temperature $T_C$ [6,9]. In these structures the minimum in free energy is shifted such that the lattice constant ratio is $c/a < 1$ in the splitting (tetragonal or orthorhombic) of the high temperature cubic austenite (AUS) phase, compared to the usual global minimum found at $c/a > 1$ in the nonmodulated tetragonal phase. Theoretical studies suggest that the modulation of the structure stabilizes this new minimum [10–12]. In $Ni_2MnGa$ compounds, we then have a situation where the interplay between an incommensurate structural modulation, a splitting of the electronic states due to the tetragonal or orthorhombic distortion of the cubic lattice and the ferromagnetic order, combine to stabilize a phase displaying a large magnetic shape-memory effect.

In this Rapid Communication we study this interplay by employing ultrafast time-resolved x-ray and optical methods to separate the three types of order in time and to investigate the possible coupling between ferromagnetism and the modulated structure. We measure a satellite reflection sensitive to the modulated structure, a (202) Bragg reflection sensitive to the orthorhombic splitting, and, optically, the change in the magnetization. This allows us to separate the fast electronic processes from thermally driven ones as we, upon photoexcitation, follow the evolution from the low temperature MT phase to the high temperature AUS phase. We quantify the relevant phonon modes and intrinsic time scales and show that while the modulation of the structure and the magnetization are quenched on the same time scale, they have different recovery times.

The 1 $\mu$m thick $Ni_{2.085}Mn_{1.133}Ga_{0.782}$ film was grown by dc-magnetron sputtering on a MgO(100) substrate with a 100 nm chromium buffer layer [13,14]. The Curie temperature is $T_C = 368$ K and the transition temperature $T_{MT}$ measured as the average of onset and completion is 349 K upon cooling and 354 K upon heating. The crystal structure of the MT phase was measured at the Material Science beamline of the Swiss Light Source [15] to be orthorhombic, with MT twinning leading to 12 different MT domains, as observed in similar films [16–18]. The MT structure is modulated [7,9,19] but unlike the single modulation wave vector $\mathbf{q} = [\xi\xi 0]$ with $\xi = 0.428$ of single crystal $Ni_2MnGa$, the film has two superimposed modulation wave vectors with $\xi = 0.311(2)$ and 0.51(1) in reciprocal lattice units of the orthorhombic lattice. The first wave vector is close to the $\xi = 0.308$ found for the 7M structure [8].

The time-resolved x-ray diffraction was performed at an x-ray energy of 5 keV using a synchrotron slicing source (200 photons/pulse, 2 kHz, and 1.2% bandwidth) as the probe and an 800 nm, 120 fs, 1 kHz $p$-polarized laser pulse at 12° incidence as the pump (absorption length $\delta = 20$ nm [20]), giving a total time resolution of 200 fs [21]. The x-ray spot was focused horizontally to 400 $\mu$m, vertically to 10 $\mu$m, and the grazing incidence angle was set to 0.65° (absorption length $\alpha = 20$ nm [22]) to match the penetration depth of the x-ray probe to the laser pump. The experiments were carried out at a sample temperature of 340 K.

*simonmariager@hotmail.com

†Also at: MAX IV Laboratory, Lund University, 22100 Lund, Sweden.

‡gerhard.ingold@psi.ch

 

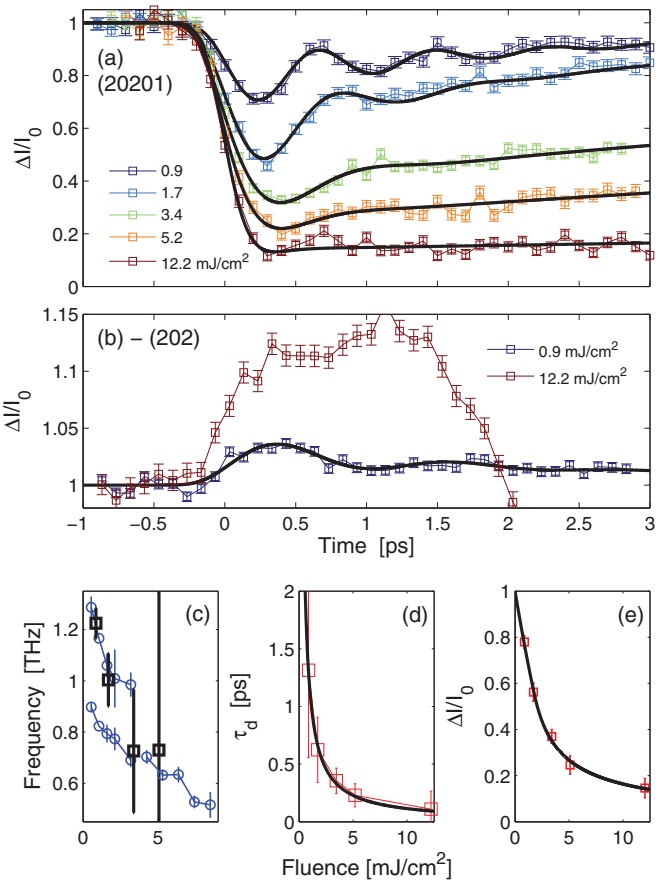


FIG. 1. (Color) Modulation dynamics. (a) Change in intensity of the (20201) satellite reflection as a function of time after laser excitation at five laser pump fluences. (b) Change in intensity of the MT (202) Bragg reflection. The color code matches (a). (c) Oscillation frequencies from optical data (circles) and the x-ray data (black squares) from (a) as a function of laser fluence. (d) Damping times from the fits in (a). (e) Intensity of the (20201) reflection after ∼500 fs. The black line is a fit as described in the text.

The time-resolved magneto-optical Kerr (TR-MOKE) effect was measured in a polar geometry with the pump laser at normal incidence (90°), the probe at 60°, and a 0.6 T magnetic field. The 80 fs, 800 nm pump and probe beams were cross polarized to minimize pump scatter. The detection was done with two balanced photodiodes and the signal was enhanced by measuring at a small heterodyne angle. The MOKE signal is found as the difference between two opposite magnetic fields and is proportional to the out-of-plane magnetization $m_z$ if in-plane dynamics and second-order terms are ignored [23].

In Fig. 1(a) we present the dynamics of the (20201) reflection, where the two extra indices label the first satellite of the (202) reflection, arising from the second modulation. At low laser pump fluences (0.9 mJ/cm$^2$ absorbed) we observe a 1.2 THz oscillation caused by a coherent optical phonon. As the fluence is increased, both the amplitude and damping of the oscillation increase, and a recovery of the intensity on a picosecond time scale is evident. At high fluence (12.2 mJ/cm$^2$) a fast drop of the intensity occurs within $\tau_e = 300 \pm 40$ fs, which roughly corresponds to a quarter of the fastest measured phonon period. At these high fluences the disappearance of the peak is a clear sign that the structural modulation is gone and that an ultrafast phase transition resulting in an increase in crystal symmetry has occurred. The fact that the intensity does not drop completely to zero can be attributed to the finite x-ray and laser penetration depths.

A structural change solely due to a change in the modulation amplitude identifies the observed coherent phonon as the amplitudon, for which the corresponding phason mode has been previously observed by neutron scattering [24]. This interpretation is supported by the measurement of the MT (202) Bragg reflection shown in Fig. 1(b). On short time scales the intensity of the (202) reflection increases, indicating an increase in orthorhombic order that is consistent with the suppression of the modulation. At low fluence (0.9 mJ/cm$^2$) a very weak oscillation appears. The drop in intensity after 1.5 ps for the data taken at 12.2 mJ/cm$^2$ is due to the thermal expansion and the MT to AUS transition. We note that if the modulation wave vectors are considered as new Γ points in the phonon dispersion curves, low lying modes in the 1 THz frequency range have also been observed in both 5M and 7M structures [25].

To quantify the observed oscillation the data of the (20201) peak was fitted with the function $I(t)/I_0 = |1 + A(\cos(2\pi\nu t)e^{-t/\tau_d} - 1)e^{-t/\tau_r}|^2$, convolved with a Gaussian function accounting for the time resolution. This function with cosine phase describes a displacive excitation [26] resulting in a damped ($\tau_d$) oscillation around a new equilibrium position ($1 - A$). The second exponential accounts for the observed recovery ($\tau_r$). This choice for $I(t)$ assumes that the x-ray structure factor is proportional to the modulation amplitude and accounts for the intensity being proportional to the square of the structure factor.

In Fig. 1(c) the frequencies obtained from the fits are plotted together with the frequencies obtained from time-resolved optical reflectivity measurements. At low fluence the x-ray and optical data are in good agreement for one of the two observed optical phonon branches while frequencies cannot be reliably extracted from the x-ray data at higher fluences. In stoichiometric $Ni_2MnGa$ single crystals we observed only a single frequency in optical experiments [27], in agreement with the existence of a single modulation wave vector [9]. In the present film sample we observe two modulation wave vectors and two frequencies. While the frequencies correspond to the excitation of two amplitudons, as observed, the (20201) reflection is only sensitive to one of these. On the other hand, the (202) peak should be sensitive to both the 0.8 and 1.2 THz oscillations, again consistent with the data.

To support the model of an amplitudon we plot the change in intensity of the (20201) reflection immediately after excitation in Fig. 1(e), extracted from the fits as $\Delta I/I_0 = (1 - A)^2$. The initial linear drop in intensity versus fluence (<2 mJ/cm$^2$) indicates a linear decrease in modulation amplitude with laser fluence, while the gradual drop at higher fluences is due to the comparable x-ray and laser penetration depths. To illustrate this we fit the fluence curve with a simple model. We assume that the transient equilibrium modulation amplitude $x$ is linear in laser fluence for $f < f_c$ and $x = 0$ for $f \geqslant f_c$. As a function of depth $z$ in the sample we write $x(z) = x_0(1 - f(z)/f_c) = x_0(1 - f_0 e^{-z/\delta}/f_c)$ for $f(z) < f_c$, where $x_0$ is the amplitude before

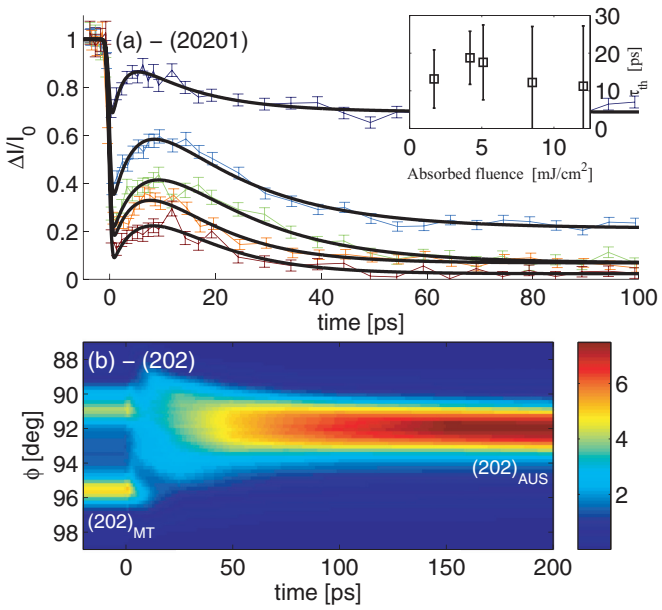


FIG. 2. (Color) MT to AUS transition. (a) Change in intensity of the (20201) satellite reflection as a function of time and laser fluence. The inset shows the thermal transition time $\tau_{\rm th}$ as a function of laser fluence. (b) Color plot of the dynamics of the (202) lattice reflection.

excitation. We then calculate the lattice sum over the lattice planes into the crystal as $S = \sum_{n_z} F(x(z))e^{2\pi i l n_z} e^{-n_z a/2\alpha}$, with the measured intensity given as $I = |S|^2$. Here $l = 2$ is the out-of-plane reciprocal lattice coordinate and $F$ is the unit cell structure factor which for a satellite reflection of an incommensurate modulation is proportional to a first-order Bessel function, $F(x) = (-1)^1 J_1(x)$ [28]. The fit then only depends on the ratio of the x-ray to laser penetration depths $\alpha/\delta$ and the critical incident fluence $f_c$. As seen in Fig. 1(e), the fit describes the data very well ($R^2 = 0.997$) with $\alpha/\delta = 1.41 \pm 0.01$ and $f_c = 1.83 \pm 0.01$ mJ/cm$^2$. We note that the fit is independent of the initial value $x_0$ in the linear regime of the Bessel function ($x_0 < 0.2$). For comparison, several other models for $x(z)$ have been tested, as outlined in the Supplemental Material [29]. To conclude, the model shows how the transient equilibrium amplitude of the modulation changes linearly with the laser excitation, which leads to a displacive excitation of the amplitude mode.

The oscillations are absent at high fluences due to the strong damping, which is shown as a function of fluence in Fig. 1(d). For the observed fluence range the damping time $\tau_d$ is inversely proportional to the fluence, as illustrated by the fit ($\tau_d = d/f$, $d = 1.14 \pm 0.05$ ps).

The ultrafast electronic quenching of the modulation is distinctly different from the slower thermally driven martensite transition. For comparison we show in Fig. 2(a) the evolution of intensity of the (20201) reflection up to 100 ps. On this time scale the initial coherent dynamics is only visible as an immediate drop in intensity, followed by a gradual recovery. This recovery is consistent with a thermalization of the electrons and the lattice, leading to a restoration of the potential which give rise to the modulation. On longer time scales a second drop in intensity occurs, which at high fluences leads to a complete quenching of the modulation. To extract the time scales the data were fitted using $I(t) = 1 - A_1 e^{-t/\tau_r} - A_2(1 - e^{-t/\tau_{\rm th}})$ accounting for the initial drop ($A_1$), the recovery ($\tau_r$), and a second exponential drop ($A_2, \tau_{\rm th}$). The weighted mean of the recovery times is $\tau_r = 4 \pm 1.7$ ps. The transition time $\tau_{\rm th}$ shown in the inset in Fig. 2(a) does not depend on the excitation fluence and has a mean value of $\tau_{\rm th} = 15 \pm 3$ ps. Due to the short x-ray absorption length the exponential drop in intensity is expected for a transition moving into the crystal at a constant speed, and nucleated MT domains are known to grow at the speed of sound [16]. The speed of sound in the [100] direction of the modulated structure is estimated to be $v \approx 5$ nm/ps [30]. A phase transition moving into the crystal at this speed would produce an exponential change in intensity with a time constant of ~7 ps. Accounting for the thermalization time between the electrons and the lattice we conclude that nucleation occurs mainly within the first 10 ps after excitation. The existence of the intermediate recovery, however, shows that the initial electronic quenching does not directly launch the final thermal phase transition.

The change in intensity of the satellite reflection can be compared to the change of the regular lattice peaks shown in Fig. 2(b). Rocking curve scans obtained at different time delays show how the (202) MT peaks transform to a single AUS (202) reflection at a pump fluence of 12.2 mJ/cm$^2$. The fast disappearance of the MT peaks is best seen at $\phi = 95.7^\circ$, where we extract a time constant of $\tau_{\rm MT} = 14 \pm 4$ ps, in agreement with the time $\tau_{\rm th}$ found for the (20201) reflection. That is, on this thermal time scale the disappearance of the MT splitting and the incommensurate modulation proceed together. The rising AUS lattice peak ($\phi = 92^\circ$) exhibits significantly slower dynamics with a rise time of 200 ps. This is due to the fact that the thin top layer directly probed by the x rays is oriented and strained by the lower part of the film. The transformation of the entire film is limited by the speed of sound, leading to a time scale of approximately $d/v \approx (1\ \mu\text{m})/(5\ \text{nm/ps}) = 200$ ps.

As pointed out above, the modulated structures only exist if $T_{\rm MT} < T_C$. This raises the question if the modulation is stabilized by an interaction between structural and magnetic order. To explore this we measured the demagnetization time after laser excitation. The TR-MOKE data at times up to 3 ps are shown in Fig. 3(a), with a reference trace measured on an Fe(001) single crystal shown for comparison in the inset. In both traces we observe a fast drop usually assigned to the demagnetization [31,32], as well as a partial recovery of the signal. The Fe trace shows a demagnetization time of $140 \pm 20$ fs and is in good agreement with previous experiments [33]. In $Ni_2MnGa$ we find a demagnetization time of $\tau_m = 320 \pm 50$ fs. Both demagnetization times were extracted by fitting the data with a step function combined with an exponential recovery. The $Ni_2MnGa$ demagnetization time is in agreement with those found for Heusler alloys with similar spin polarization factors, though these were measured in spintronic compounds with AUS structures [34,35]. We thus find that the demagnetization and the quenching of the structural modulation occur essentially simultaneously. If we instead measure the time evolution up to 50 ps as shown in Fig. 3(c), the TR-MOKE data does not show an intermediate

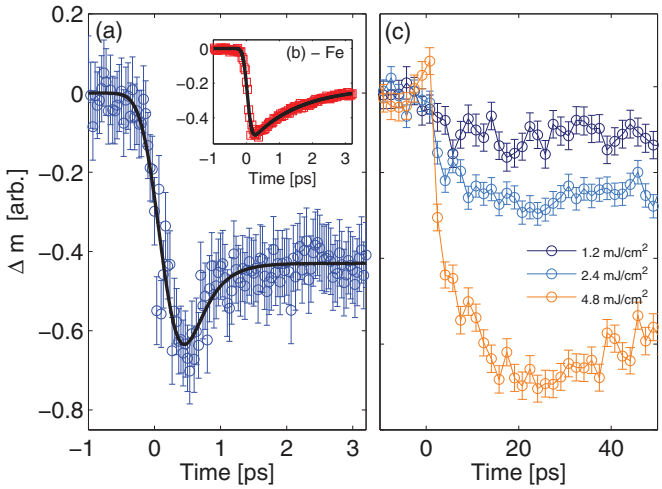


FIG. 3. (Color) Magnetization dynamics. (a) Change in magnetization as a function of time for $Ni_2MnGa$. The pump fluence was 1.4 mJ/cm$^2$. (b) Reference trace taken on an Fe(001) single crystal. (c) Change in magnetization for $Ni_2MnGa$ at times up to 50 ps for three different fluences.

recovery, unlike the structural data in Fig. 2(a). We conclude that the magnetization and the structural modulation have different dynamics after the initial drop. The modulation therefore cannot be stabilized by a direct coupling to the magnetic moment, though they are both rapidly quenched after the laser excitation of the electronic subsystem.

Upon laser excitation several time scales are present in $Ni_2MnGa$. The structural modulation is fully quenched within 300 fs, about a quarter of the corresponding phonon period. The ferromagnetic order is quenched with a demagnetization time of 320 fs and the MT to AUS transition occurs after thermalization of the electron and lattice (∼4 ps) with nucleation within 10 ps and the subsequent domain growth limited by the speed of sound. These time scales are independent of the excitation fluence and intrinsic to the system. The fact that the ultrafast structural transition appears before thermalization between the electrons and the lattice, and recovers upon thermalization despite the demagnetization indicates that the origin of the incommensurate modulation is the strong electron phonon interaction. A possible explanation is the destabilization of the incommensurate modulation by distortion of the Kohn anomaly [10] near the Fermi edge via excitation of Ni 3*d* electrons to unoccupied states just above the Fermi edge. Such states are available in both minority and majority bands [36,37], and the importance of Ni 3*d* states for the structural transitions in $Ni_2MnGa$ has been previously outlined [13]. An alternative mechanism could involve destruction of the suggested hybrid bonding between Ni *d* and Mn *p* states near the Fermi level [11,38]. On the other hand, the quenching of both the modulation and the magnetism does not lead directly to the MT transition. The transition only occurs when a temperature above $T_{MT}$ has been reached and all subsystems are in thermal equilibrium.

To summarize, we measured a coherent phonon mode and an ultrafast nonthermal structural transition in an incommensurately modulated $Ni_2MnGa$ film. Both the observation of this phase transition and the displacive excitation of the phonon is consistent with the concept of an amplitudon. The dynamics of this electronically driven ultrafast transition is distinctly different from the much slower thermally driven martensite transition, which proceeds with nucleation within 10 ps and domain growth limited by the speed of sound. The different recoveries of the demagnetization and the structural modulation indicates that the origin of the modulation is electronic. This example shows how ultrafast pump-probe methods applying a variety of specific probes can be used to disentangle the different degrees of freedom in multiferroic materials.

The x-ray experiments were performed on the X04SA and X05LA beamlines of the Swiss Light Source, Paul Scherrer Institut, Villigen, Switzerland. We thank P. Willmott, D. Grolimund, and C. Borca for help. This work was supported by the Swiss National Foundation through NCCR MUST, by the DFG through SPP 1239 within Ja821/3-3, and by the Graduate School of Excellence Materials Science in Mainz (MAINZ).

[1] A. Planes, L. Maosa, and M. Acet, J. Phys.: Condens. Matter **21**, 233201 (2009).
[2] T. Graf, C. Felser, and S. S. Parkin, Prog. Solid State Chem. **39**, 1 (2011).
[3] K. Ullakko, J. K. Huang, C. Kantner, R. C. O'Handley, and V. V. Kokorin, Appl. Phys. Lett. **69**, 1966 (1996).
[4] S. J. Murray, M. Marioni, S. M. Allen, R. C. O'Handley, and T. A. Lograsso, Appl. Phys. Lett. **77**, 886 (2000).
[5] A. Sozinov, A. A. Likhachev, N. Lanska, and K. Ullakko, Appl. Phys. Lett. **80**, 1746 (2002).
[6] N. Lanska, O. Söderberg, A. Sozinov, Y. Ge, K. Ullakko, and V. K. Lindroos, J. Appl. Phys. **95**, 8074 (2004).
[7] L. Righi, F. Albertini, L. Pareti, A. Paoluzi, and G. Calestani, Acta Mater. **55**, 5237 (2007).
[8] L. Righi, F. Albertini, E. Villa, A. Paoluzi, G. Calestani, V. Chernenko, S. Besseghini, C. Ritter, and F. Passaretti, Acta Mater. **56**, 4529 (2008).
[9] S. Mariager, T. Huber, and G. Ingold, Acta Mater. **66**, 192 (2014).
[10] C. Bungaro, K. M. Rabe, and A. Dal Corso, Phys. Rev. B **68**, 134104 (2003).
[11] A. T. Zayak and P. Entel, Mater. Sci. Eng., A **378**, 419 (2004).
[12] P. Entel, M. Siewert, M. E. Gruner, H. C. Herper, D. Comtesse, R. Arroyave, N. Singh, A. Talapatra, V. V. Sokolovskiy, V. D. Buchelnikov *et al.*, Eur. Phys. J. B **86**, 65 (2013).
[13] G. Jakob, T. Eichhorn, M. Kallmayer, and H. J. Elmers, Phys. Rev. B **76**, 174407 (2007).
[14] T. Eichhorn, R. Hausmanns, and G. Jakob, Acta Mater. **59**, 5067 (2011).
[15] P. R. Willmott, D. Meister, S. J. Leake, M. Lange, A. Bergamaschi, M. Böge, M. Calvi, C. Cancellieri, N. Casati, A. Cervellino *et al.*, J. Synchrotron Radiat. **20**, 667 (2013).
[16] A. G. Khachaturyan, *Theory of Structural Transformations in Solids* (Wiley, New York, 1983).

[17] P. Klaer, T. Eichhorn, G. Jakob, and H. J. Elmers, Phys. Rev. B **83**, 214419 (2011).
[18] T. Eichhorn, R. Hausmanns, P. Klaer, M. Kallmayer, H.-J. Elmers, and G. Jakob, Adv. Eng. Mater. **14**, 687 (2012).
[19] A. Zheludev, S. M. Shapiro, P. Wochner, and L. E. Tanner, Phys. Rev. B **54**, 15045 (1996).
[20] Y. Zhou, X. Jin, H. Xu, Y. V. Kudryavtsev, Y. P. Lee, and J. Y. Rhee, J. Appl. Phys. **91**, 9894 (2002).
[21] P. Beaud, S. L. Johnson, A. Streun, R. Abela, D. Abramsohn, D. Grolimund, F. Krasniqi, T. Schmidt, V. Schlott, and G. Ingold, Phys. Rev. Lett. **99**, 174801 (2007).
[22] B. L. Henke, E. M. Gullikson, and J. C. Davis, At. Data Nucl. Data Tables **54**, 181 (1993).
[23] C.-Y. You and S.-C. Shin, Appl. Phys. Lett. **69**, 1315 (1996).
[24] S. M. Shapiro, P. Vorderwisch, K. Habicht, K. Hradil, and H. Schneider, Europhys. Lett. **77**, 56004 (2007).
[25] S. Ener, T. Mehaddene, B. Pedersen, M. Leitner, J. Neuhaus, and W. Petry, New J. Phys. **15**, 123016 (2013).
[26] H. J. Zeiger, J. Vidal, T. K. Cheng, E. P. Ippen, G. Dresselhaus, and M. S. Dresselhaus, Phys. Rev. B **45**, 768 (1992).
[27] S. O. Mariager, A. Caviezel, P. Beaud, C. Quitmann, and G. Ingold, Appl. Phys. Lett. **100**, 261911 (2012).
[28] S. V. Smaalen, *Incommensurate Crystallography* (Oxford University Press, Oxford, U.K., 2007).
[29] See Supplemental Material at http://link.aps.org/supplemental/10.1103/PhysRevB.90.161103 for additional information given on our static x-ray diffraction measurements to determine the crystal structure, on our optical reflectivity measurements to clarify the nature of the phonon modes, and on the time-resolved rocking curves to trace the structural evolution of the laser induced phase transition up to 300 ps for different laser fluences.
[30] C.-M. Li, H.-B. Luo, Q.-M. Hu, R. Yang, B. Johansson, and L. Vitos, Phys. Rev. B **84**, 174117 (2011).
[31] A. Kirilyuk, A. V. Kimel, and T. Rasing, Rev. Mod. Phys. **82**, 2731 (2010).
[32] G. Malinowski, F. D. Longa, J. H. H. Rietjens, P. V. Paluskar, R. Huijink, H. J. M. Swagten, and B. Koopmans, Nat. Phys. **4**, 855 (2008).
[33] T. Kampfrath, R. G. Ulbrich, F. Leuenberger, M. Münzenberg, B. Sass, and W. Felsch, Phys. Rev. B **65**, 104429 (2002).
[34] D. Steil, S. Alebrand, T. Roth, M. Krauß, T. Kubota, M. Oogane, Y. Ando, H. C. Schneider, M. Aeschlimann, and M. Cinchetti, Phys. Rev. Lett. **105**, 217202 (2010).
[35] A. Mann, J. Walowski, M. Münzenberg, S. Maat, M. J. Carey, J. R. Childress, C. Mewes, D. Ebke, V. Drewello, G. Reiss, and A. Thomas, Phys. Rev. X **2**, 041008 (2012).
[36] S. R. Barman, S. Banik, and A. Chakrabarti, Phys. Rev. B **72**, 184410 (2005).
[37] C. P. Opeil, B. Mihaila, R. K. Schulze, L. Mañosa, A. Planes, W. L. Hults, R. A. Fisher, P. S. Riseborough, P. B. Littlewood, J. L. Smith *et al.*, Phys. Rev. Lett. **100**, 165703 (2008).
[38] J. Kübler, A. R. Williams, and C. B. Sommers, Phys. Rev. B **28**, 1745 (1983).